JOURNAL OF THERMOPHYSICS AND HEAT TRANSFER
Vol. 17, No. 1, January–March 2003

Membrane Formation Process in Magnetic Fluid and Application for Aperture Control

H. Yamaguchi,* Y. Suzuki,† and S. Shuchi‡
Doshisha University, Kyoto 610-0321, Japan

Basic characteristics of the membrane formation process were investigated experimentally and numerically. In the experiment the aperture area of magnetic fluid membrane was recorded for a given volume of magnetic fluid sustained by applying a magnetic field in a pipe section. In the numerical analysis the formation process of the magnetic fluid membrane was examined under various magnetic field intensities. The theoretical background of the numerical work is based on the static force balance between gravity, magnetic force density, and surface tension on the membrane at the solid contact point. The surface profile was estimated at an equilibrium stage by numerical analysis and compared to experimental results, where the membrane (sustained by magnetic fluid in a pipe) formed the aperture configuration. In the results of the present investigation, from both experimental and numerical work, the detailed formation process was verified, and it was shown that the aperture area can be controlled by applying a magnetic field.

Nomenclature

$\boldsymbol{F}$	=	body force density, N/m^3
$\boldsymbol{f}_g$	=	gravitational body force density, N/m^3
$\boldsymbol{f}_m$	=	Kelvin body force density, N/m^3
$\boldsymbol{f}_s$	=	surfacial force density, N/m^3
g	=	gravitational acceleration, m/s^2
H	=	magnetic field intensity, A/m
$\boldsymbol{H}$	=	magnetic field vector
H_r	=	intensity of magnetic field on r direction, A/m
H_z	=	intensity of magnetic field on z direction, A/m
H_z^*	=	nominal value of H_z; the maximum of H_z, A/m
I	=	applied dc current, A
k	=	Boltzmann constant
M	=	magnetization, Wb/m^2
$\boldsymbol{M}$	=	magnetization vector, Wb/m^2
M_S	=	saturation magnetization, Wb/m^2
R	=	surface curvature at interface
R_s	=	representative surface curvature at solid contact
r, θ, z	=	cylindrical coordinates (see Fig. 3), -
S	=	aperture area, m^2
T	=	absolute temperature, K
$\hat{\boldsymbol{t}}$	=	tangential unit vector
V_i	=	volume of iterated step magnetic fluid, m^3
V_m	=	volume of sustained magnetic fluid, m^3
x, y, z	=	Cartesian coordinates
η_0	=	viscosity, Pa s
ρ	=	relative density, kg/m^3
ρ_0	=	reference density; magnetic fluid, kg/m^3
ρ'	=	contact fluid density, kg/m^3
σ	=	surface tension, N/m
φ	=	contact angle, rad

Received 18 March 2002; revision received 8 July 2002; accepted for publication 13 July 2002.

*Professor, Department of Mechanical Engineering; hyamaguc@mail.doshisha.ac.jp.

†Research Student, Department of Mechanical Engineering; eta1305@mail4.doshisha.ac.jp.

‡Research Student, Department of Mechanical Engineering; dta0379@mail4.doshihsa.ac.jp.

I. Introduction

A MAGNETIC fluid is a suspension of very fine magnetic particles with typical size of the order of 10 nm in a carrier liquid. It has a unique character in a magnetic field, and it behaves like a magnetized liquid. To date, using such a unique character of a magnetic fluid, there are many engineering applications thought of and proposed, and some of applications,[1] such as seals and sensors,[2] have already materialized or become realistic industrial products.[3,4] The field of applications of magnetic fluids is still expanding, and new ideas of applications are actively emerging.

The interfacial phenomena of a magnetic fluid, such as spike phenomena,[5] have been reported for many years since the first appearance of magnetic fluid. However, so far there are few applications for the unique interfacial formation[6,7] of magnetic fluid, and hence more detailed study of the interfacial phenomena is required. The liquid column formation is another interesting phenomenon in the basic fluid mechanics[8–10] and in an application for the crystal growth technology.[11] For a magnetic fluid column Ohaba et al.[12] have varied vibration properties for a vertically oscillating magnetic fluid column and commented on a possible application for a crystal growth (columns) in a microgravity environment. Although there have been some attempts to study the magnetic fluid columns in an engineering application, there has been no work to examine a possibility of flow control (aperture control) and to verify basic properties for the magnetic fluid columns sustained in a section of circular pipe yet.

In the present study the unique feature of membrane formation is examined, and a feasibility study is given for a new way of aperture control, which utilizes sustained magnetic fluid in a pipe by an applied magnetic field. The basic idea, using the sustained magnetic fluid in a section of pipe, is to form the membrane and block the passage by controlling magnetic field intensity. In the present investigation basic characteristics of the membrane formation are investigated experimentally, using water-based magnetic fluid (W-40) with the contact fluids of air and mineral oil. In the experiment the aperture area of a magnetic fluid membrane is recorded for a given volume of magnetic fluid sustained in a pipe section by varying magnetic field intensity. A numerical analysis for studying the formation process of a membrane of magnetic fluid by applying magnetic field is also conducted in the present study. The theoretical background of the numerical work is based on the static force balance between the gravity, magnetic force density, and surface tension on the membrane at the solid contact point. The surface profile is obtained at an equilibrium stage, where the membrane (sustained by magnetic fluid in a pipe) forms an aperture configuration.

In view of application for aperture control, particularly in the present study, attention was given to investigating detailed characteristics of aperture area variation in terms of imposed magnetic field intensity.

II. Experimental Apparatus and Procedure

Figure 1 is a schematic diagram of the experimental apparatus. A volume of magnetic fluid is sustained by magnetic field in the test section, which is made of acrylic pipe of inner diameter 12 mm with total length of 800 mm. At both ends of the test section, reservoir tanks are attached so that contact fluid (mineral oil or air) can be contained in a static state and filling the section. A coil electromagnet is placed around the test section and is cooled by circulating water from a cooler unit. The electromagnet is powered by a dc power supply unit, which could produce the magnetic field strength of $0 \sim 0.5 \times 10^5$ A/m in the test section. The aperture area of the magnetic fluid membrane, when the magnetic field is imposed, is measured by a video image, which is taken by a high-resolution video camera with lighting at one end of the reservoir tanks and is monitored and processed digitally.

In Fig. 2 details of the test section are shown. Experiments were conducted by filling the contact fluid (in the case of oil) in the reservoir tanks at a given level, and then a given volume of magnetic fluid was pushed into the test section by a syringe through the filling stainless pipe, as shown in Fig. 2, while applying an appropriate magnetic field to sustain the magnetic fluid in the test section. Experiments were carried out in a temperature-controlled room so that contact fluids (oil or air) with magnetic fluid membrane were kept at constant temperature at 25°C (±1°C). For a given volume of magnetic fluid, the magnetic field intensity was varied. In the present study the external magnetic field was imposed on the magnetic fluid membrane in the test section by the solenoid-type coil electromagnet. Prior to experiments with the membrane formation, detailed data were taken for magnetic field distribution in the test section by supplying dc electric power to the electromagnet. In Fig. 3 a schematic diagram to describe the sustained magnetic fluid membrane is shown, where the cylindrical coordinates are presented as well. The origin of the coordinate system, as shown in Fig. 3, is taken at the center of electromagnet on the axis of the pipe in the test section. In Fig. 4 representative distributions of the magnetic field intensity in the test section are plotted in Fig. 4 for the axial component H_z and in Fig. 5 for the radial component H_r, when a typical dc current of $I = 100$ mA was applied to the magnet. It

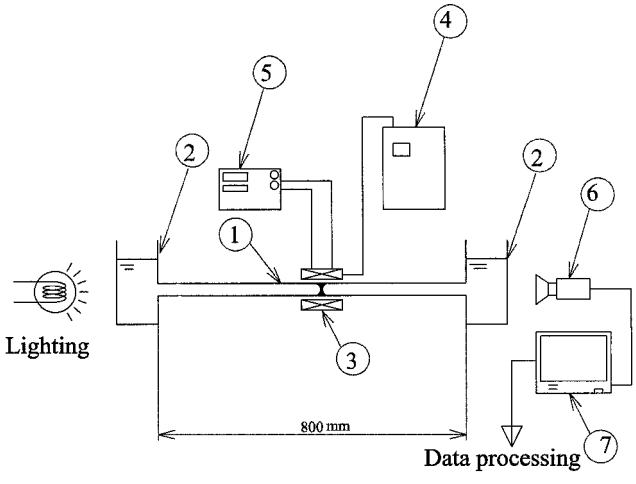

Fig. 1 Experimental apparatus: 1, test section; 2, reservior tank; 3, electromagnet; 4, cooler; 5, dc power supply; 6, video camera (CCD); and 7, monitor.

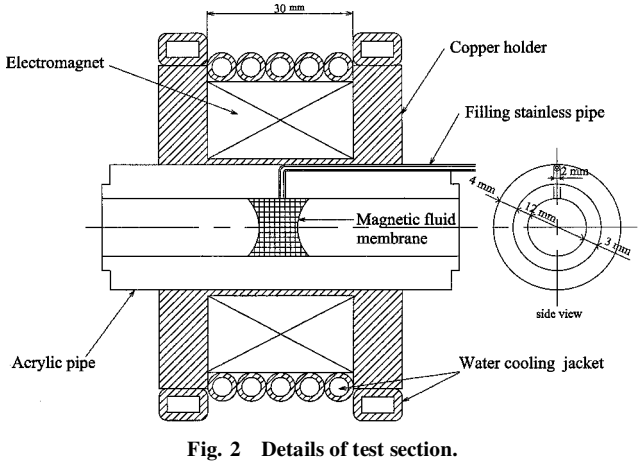

Fig. 2 Details of test section.

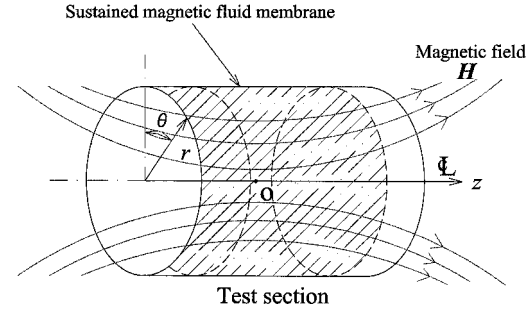

Fig. 3 Cylindrical coordinate system for applied magnetic field.

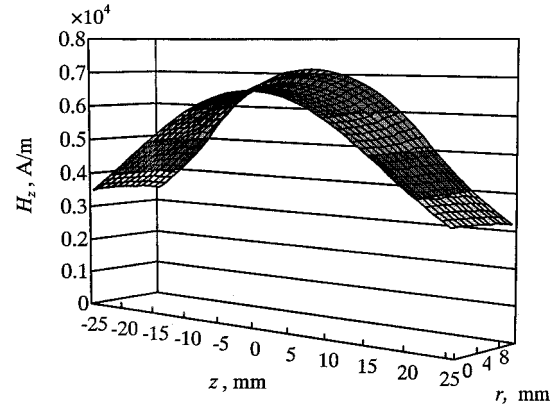

Fig. 4 Distribution of magnetic field: H_z component of H.

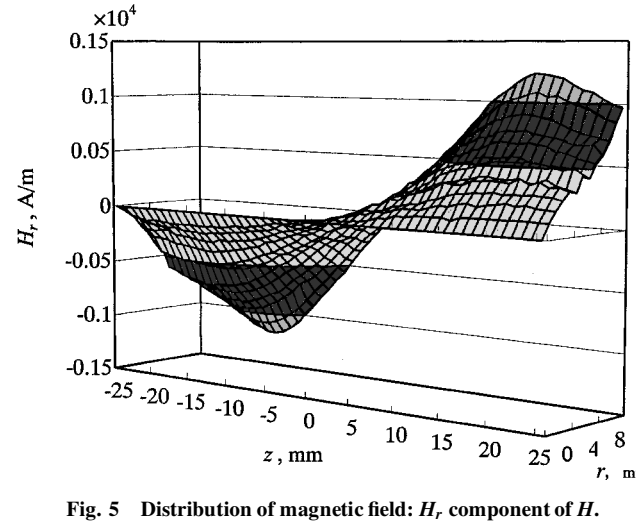

Fig. 5 Distribution of magnetic field: H_r component of H.

Table 1 Properties of test fluids at 25°C

Test fluid	Density ρ, kg/m^3	Viscosity η_0, Pa · s
Air	1.184	18.2×10^{-6}
Mineral oil SM-2	0.382×10^3	1.86×10^{-3}
Magnetic fluid W-40	1.407×10^3	30×10^{-3}

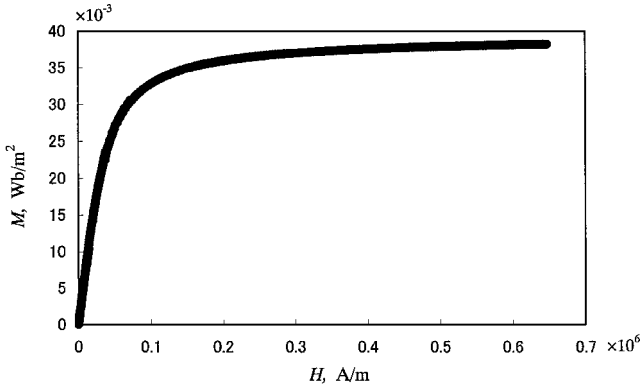

Fig. 6 Magnetization characteristics of magnetic fluid (W-40).

is mentioned that the magnetic field is axisymmetric because the magnetic field was generated by the solenoid coil electromagnet. As seen in Figs. 4 and 5, there is a smooth and symmetric magnetic field, whose peak value exists at $z = 0$ for H_z (which varies for r direction and zero value of H_r at $z = 0$, $r = 0$).

Magnetic fluid used in the present investigation is water-based magnetic fluid (W-40) as supplied by industry. The magnetization characteristic is displayed in Fig. 6. The magnetization characteristic of the magnetic fluid (W-40) is fairly well known in literature,[13] so that in the present study it is characterized by the Langevin function.[14]

The contact fluids are primarily air and a mineral oil (SM-2) supplied by industry. The mineral oil has excellent separativeness from the magnetic fluid and forms a clear interfacial surface. The basic physical properties of the contact fluids are tabulated in Table 1.

The initial measurement error for determining the surface profile and aperture area comes from the resolution accuracy of the high-resolution video camera. The camera has 1.23×10^6 pixels in charge-coupled device (CCD) image receiving. The digital image is then processed by an image processor in an accuracy of within ±1% (implies to the instrumentation accuracy). However, in capturing the images (the surface profile on aperture area), light refraction (scattering) on the interface occurs and gives somewhat vague digital images of CCD output. For extremely vague images of CCD output, the profile of interfacial surface was traced manually in comparison with direct visual images and then sent to the image processing. This image-processing procedure was repeated several times to minimize the error. Resultantly, the surface profile and the aperture area presented in the present study involve the overall error (after the image processor) of approximately maximum ±5.0%.

III. Numerical Analysis

The surface profile of the membrane formed in the test section, where the magnetic field is applied with various intensities, is calculated numerically by solving the equilibrium equation of force balance between the magnetic body force, gravity force, and surface tension. The equilibrium equation of force balance can be written as

$$\boldsymbol{F} = \boldsymbol{f}_m + \boldsymbol{f}_g + \boldsymbol{f}_s \tag{1}$$

where $\boldsymbol{f}_m$ is the Kelvin body force density,[1–3] $\boldsymbol{f}_m = (\boldsymbol{M} \cdot \nabla)\boldsymbol{H}$, $\boldsymbol{f} = \rho \boldsymbol{g}$, and $\boldsymbol{f}_S = \sigma(1/R_S)\hat{\boldsymbol{t}}$.

Considering the membrane in the cylindrical coordinate system of Fig. 3, components in each coordinate direction r, θ, z of the force

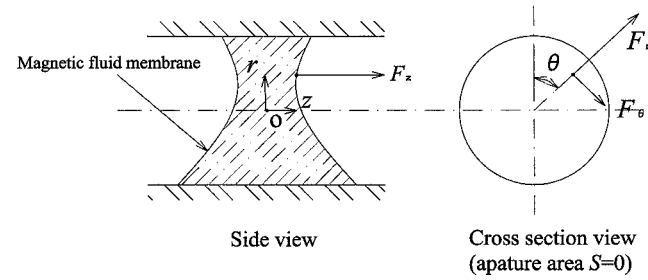

Fig. 7 Body force balance.

$\boldsymbol{F}$ in Eq. (1) can be written as follows, referring to the schematic diagram of Fig. 7:

$$F_r = M_r \frac{\partial H_r}{\partial r} + M_z \frac{\partial H_r}{\partial z} - \rho g \cos\theta + f_S \sin\varphi \tag{2}$$

$$F_\theta = -\rho g \sin\theta \tag{3}$$

$$F_z = M_r \frac{\partial H_z}{\partial r} + M_z \frac{\partial H_z}{\partial z} + f_S \cos\varphi \tag{4}$$

where the magnitude of magnetization $\boldsymbol{M}$ of the magnetic fluid is approximated by following Langevin function[14] (Fig. 6):

$$\boldsymbol{M} = M_S L(mH/kT) \tag{5}$$

$$L(x) = \coth x - 1/x \tag{6}$$

In the present study setting $x = mH/kT$ for the given temperature $T = 298$ K, x can be expressed from known characteristics of Fig. 6. Thus, using Eqs. (2–6) the following ordinary differential equation of force balance is obtained:

$$F_r\,\mathrm{d}r + F_\theta r\,\mathrm{d}\theta + F_z\,\mathrm{d}z = \Delta p \tag{7}$$

where on the surface of membrane, that is, on the interfacial surface, the pressure difference Δp can be set as $\Delta p = 0$. For magnetic field $\boldsymbol{H}(H_r, H_\theta, H_z)$ in Eqs. (2–4), measured values (as representationally shown in Figs. 4 and 5) are employed in the calculation, adopting the axisymmetric condition that $H_\theta = 0$. It is noted that ρ in Eqs. (2) and (3) are the relative density, which can be defined by $\rho = \rho_0 - \rho'$.

In the numerical calculation to obtain the surface profile of the membrane, the following integration was performed by Simpson's method:

$$\int F_r\,\mathrm{d}r + \int F_\theta r\,\mathrm{d}\theta + \int F_z\,\mathrm{d}z = C \tag{8}$$

where C is the integral constant. The surface tension is only considered at the solid contact point, where the contact angle φ between the magnetic fluid membrane surface and pipe wall was assumed as $\varphi = 150$ deg. The contact angle of $\varphi = 150$ deg was adopted from a separate experimental observation (drop test) for a drop of magnetic fluid on an acrylic sheet. Furthermore, the surface tension force f_S is only calculated at the contact point, as $f_S = \sigma(1/R_S)$, where the curvature R_S of the membrane surface is also assumed at the contact surface as $R_S = 1$ mm from the drop test. The actual value of σ (under effect of magnetic field) is very difficult to determine, and in the present investigation the value of σ is simply adopted as typical value from Ref. 1. In the present investigation the surface tension on the interfacial surface was neglected, apart from the contact point (at the pipe wall), because the effect of the surface tension on the interfacial surface is approximately within ±1% from the effect of other forces and the curvature R cannot be known a priori. Thus, the most essential effect of the surface tension is the effect at the solid contact with the pipe wall.

To obtain the surface profile (the interfacial deformation profile), the integral constant C in Eq. (8) was determined so that the given volume V_m (actual sustained volume) of the magnetic fluid is the same as the volume content V_i (i is the number of iteration steps)

confined in the calculated surface profiles. The numerical sequence was continued, until $|V_i - V_m| \leq e$, [typically e is the convergence criteria ($e = 1 \times 10^{-6}$)], by the successive iteration starting from an appropriate initial value of C. It is mentioned that V_m is the important parameter to determine the surface profile.

The accuracy of the calculation is mostly depending on the measurement accuracy of the magnetic field (Figs. 4 and 5). The distribution of the magnetic field intensity was measured by a Hall probe, whose instrumentation accuracy is within $\pm 1\%$ for the range of the magnetic field intensity. However, the largest measurement error comes from positioning the Hall probe in the measuring space, which was achieved by constructing a procession stage. The margin of error associated with the measurement of the magnetic field intensity is approximately maximum $\pm 4.0\%$. The procedure of the measurement (positioning the Hall probe) was repeated for several times to minimize the error. The data shown in Figs. 4 and 5 are the average values from repeated measurements.

IV. Results and Discussion

In Figs. 8–11, representative surface profiles for the case of an air-magnetic fluid interface of the membrane at a given magnetic field intensity H_z^* are displayed for a sustained volume $V_m = 3.00$ ml. H_z^* is the nominal value, which is the maximum intensity of the applied magnetic field. In each profile for a given H_z^*, the frontal view (y–z plane) and the cross-sectional view (r–θ plane) are displayed, for example, at $H_z^* = 0.461 \times 10^5$ A/m, Figs. 8a and b, respectively. Also, in each profile for a given H_z^*, estimated results from the numerical analysis and the location of membrane surface are shown as a solid line and are compared to the experimental data in Figs. 8a, 9a, 10a, and 11a, and Figs. 8b, 9b, 10b, and 11b. The shaded area in the cross-sectional view in each profile (Figs. 8b, 9b, 10b, and 11b) are images obtained from the experimental observations (images obtained from the high-resolution video camera), and again the estimated results from the numerical analysis are superimposed by the solid line. As seen in Figs. 8 and 9 at relatively high magnetic fields, the membrane formed by the sustained magnetic fluid blocks the pipe in the test section, and at the upper wall, because of the surface tension at the contact points, the membrane forms a concave shape (Figs. 8a and 9a). As the membrane surface approaches the

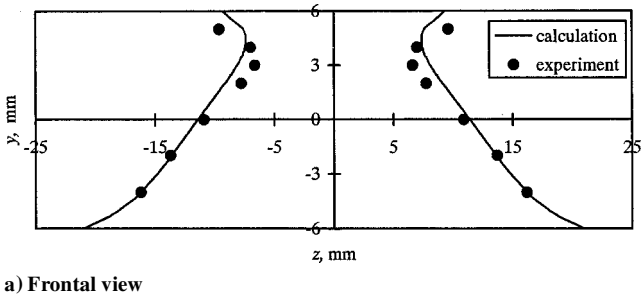

a) Frontal view

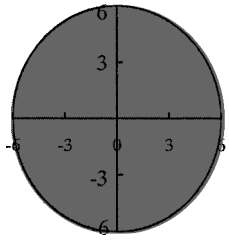

b) Cross-sectional view

Fig. 8 Surface profile of membrane ($V_m = 3.00$ ml) for air-magnetic fluid interface for $H_z^* = 0.461 \times 10^5$ A/m.

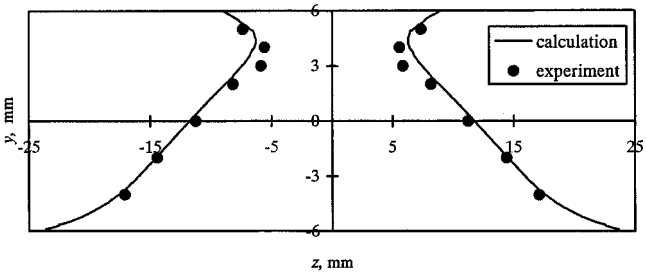

a) Frontal view

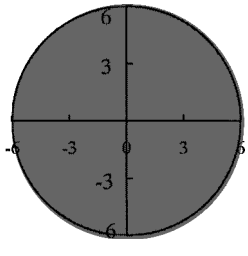

b) Cross-sectional view

Fig. 9 Surface profile of membrane ($V_m = 3.00$ ml) for air-magnetic fluid interface for $H_z^* = 0.395 \times 10^5$ A/m.

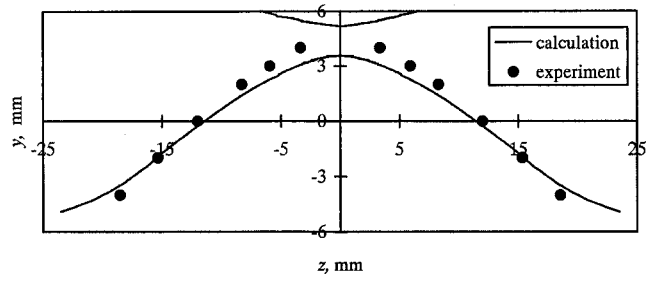

a) Frontal view

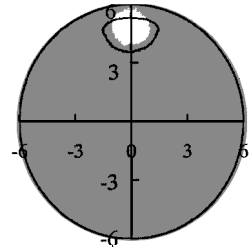

b) Cross-sectional view

Fig. 10 Surface profile of membrane ($V_m = 3.00$ ml) for air-magnetic fluid interface for $H_z^* = 0.313 \times 10^5$ A/m.

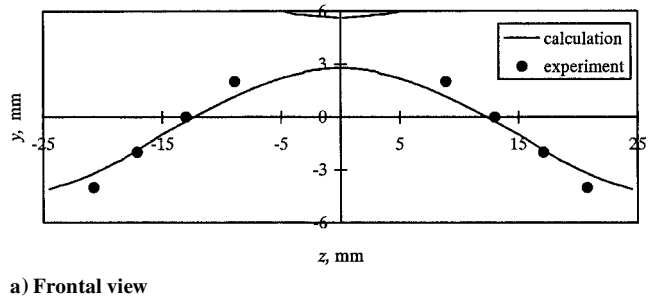

a) Frontal view

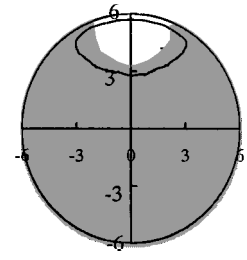

b) Cross-sectional view

Fig. 11 Surface profile of membrane ($V_m = 3.00$ ml) for air-magnetic fluid interface for $H_z^* = 0.264 \times 10^5$ A/m.

lower wall, the thickness of the membrane increases as a result of the gravity that balances the magnetic body force. However, when the magnetic field intensity H_z^* is lowered the aperture areas (cross-sectional opening area in membrane as recorded by the video image in Fig. 1) start to appear in the membrane, as seen in Figs. 10a and 10b. The aperture area tends to appear adjacent to the upper wall, when the concavity of the membrane reached the minimum thickness. (The detailed formation process will be discussed fully in a following paragraph.) Further decrease of the magnetic field intensity results in opening a larger aperture area, as seen in Figs. 11a and 11b.

As seen in Figs. 8–11, fair agreement between the estimated surface profiles from the numerical analysis and the experimental data has been reached. The deviation between the numerical results and the experimental measurements was caused by conditions at the wall contact, where the curvature and contact angle were assumed constants as explained earlier. Similar phenomena occurred with the oil-magnetic fluid interface, although the applied magnetic field intensity is lower than in the case of the air-magnetic fluid interface for a given aperture area. This is mainly because of the density of fluids and the difference of the contact condition (surface tension effect). Thus, from experimental results, which were verified analytically in Figs. 8–11, it is shown that aperture control is possible by alternating the applied magnetic field intensity. The detail of the variation of aperture area for air-magnetic fluid and oil-magnetic fluid cases are discussed in the following paragraph for Figs. 12–14.

In Figs. 12 and 13 variation of the aperture area for each given volume of magnetic fluid is depicted as the nominal magnetic field intensity H_z^* is increased from the minimum sustainable magnetic field intensity. In Fig. 12 the results for the air-magnetic fluid interface and in Fig. 13 the results for the oil-magnetic fluid interface are displayed for sustained volumes ranging from $V_m = 1.00 \sim 3.50$ ml. From the results in Figs. 12 and 13, it is seen that the aperture area decreases as the magnetic field intensity is increased, as already described in Figs. 8–11, for each given volume of magnetic fluid sustained in the test section. However, for $V_m = 1.00 \sim 2.50$ ml in Fig. 12 and for $V_m = 1.00 \sim 2.00$ ml in Fig. 13, the aperture area did not reach zero, that is, total blocking of the test section was not achieved within the range of magnetic field intensity in the present study. On the other hand, when the volume is increased such that $V_m \geq 3.00$ ml in Fig. 12 and $V_m \geq 2.50$ ml in Fig. 13 the aperture closes (the opening area disappears) and blocks the test section completely when the magnetic field intensity increases, as seen in Figs. 12 and 13. The volume dependency for the variation of aperture area in Figs. 12 and 13 is caused by the relative force balance between the magnetic body force and gravitational force along the magnetic field lines. Increasing the volume of the sustained magnetic fluid causes higher pressure at lower wall region (toward the direction of gravity) by the gravity force in the test section, which has to be balanced by the higher magnetic body force to sustain the membrane. In the comparison between Figs. 12 and 13, because of the buoyancy effect, which comes from the difference of the fluid densities (air and oil), less magnetic body force (less magnetic field intensity) is required to sustain the membrane for oil-magnetic fluid interface, when compared to the same aperture area of the air-magnetic fluid interface.

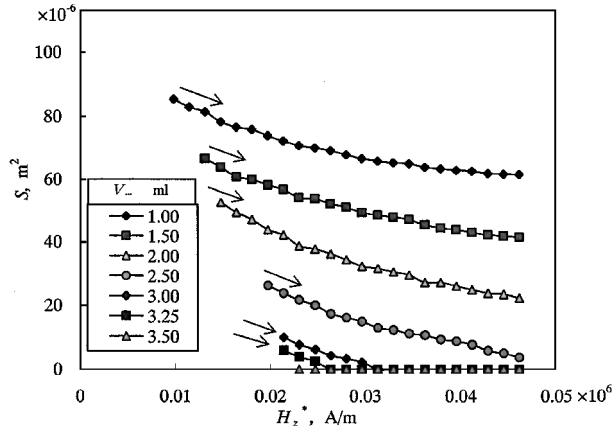

Fig. 12 Variation of aperture area with increasing H_z^* for air-magnetic fluid interface.

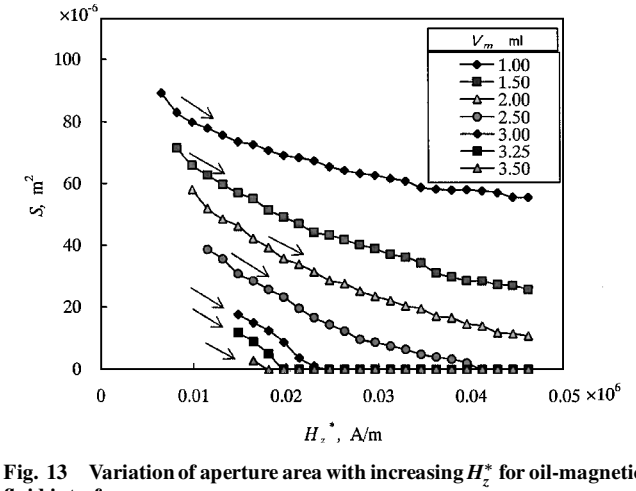

Fig. 13 Variation of aperture area with increasing H_z^* for oil-magnetic fluid interface.

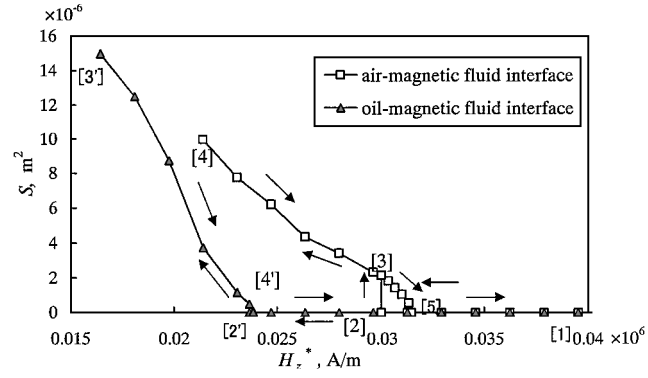

Fig. 14 Hysteresis loop ($V_m = 3.00$ ml).

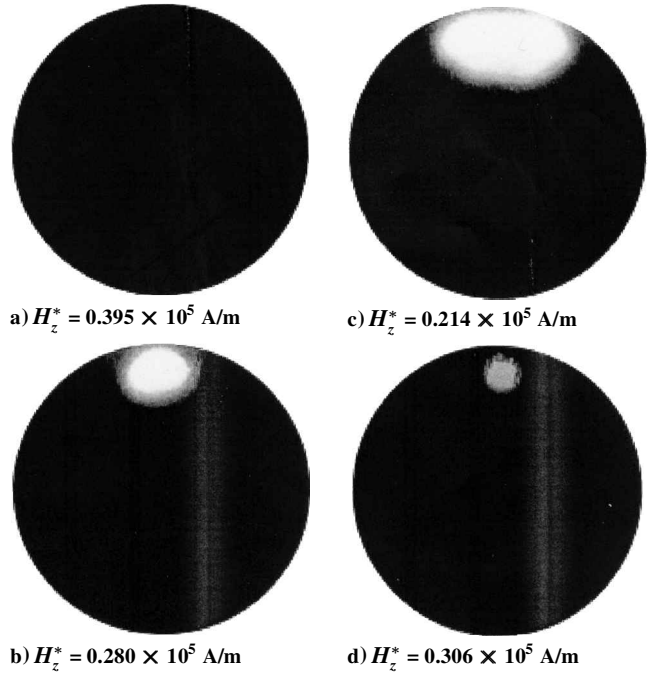

a) $H_z^* = 0.395 \times 10^5$ A/m **c) $H_z^* = 0.214 \times 10^5$ A/m**

b) $H_z^* = 0.280 \times 10^5$ A/m **d) $H_z^* = 0.306 \times 10^5$ A/m**

Fig. 15 Representative images of aperture area for air-magnetic fluid interface for values H_z^* in Fig. 14.

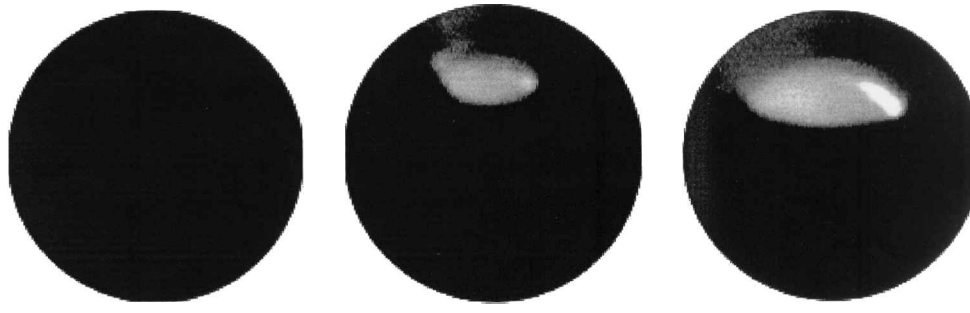

a) $H_z^* = 0.395 \times 10^5$ A/m b) $H_z^* = 0.214 \times 10^5$ A/m c) $H_z^* = 0.165 \times 10^5$ A/m

Fig. 16 Representative images of aperture area for oil-magnetic fluid interface for values H_z^* in Fig. 14.

An analytical attempt was made to estimate the variation of aperture area in terms of the changing magnetic field intensity shown in Fig. 12. The results obtained from the numerical analysis did not give a correct estimate for the experimental data shown in Fig. 12. This is mainly a result of the condition at the contact point on the solid pipe wall because in the present study the contact angle and curvature at the contact point were assumed constant and their value were taken from the drop test. The difference could be seen in Figs. 10 and 11, where the estimated numerically calculated results of the solid lines deviated from the experimental observation. This would clearly give the limitation of the present numerical analysis, although the formation process of the surface profiles of the membrane (Figs. 8–11) were well presented and explained.

To further study controlling the aperture area, experiments were conducted, where the procedure of increasing the magnetic field intensity was reversed and altered to descending order of magnetic field intensity in the experiment. In Fig. 14 representative cases of variation of aperture area are depicted for the air-magnetic fluid interface and oil-magnetic fluid interface with a given sustained volume of membrane $V_m = 3.00$ ml. In Figs. 15 and 16 some representative CCD images (taken from the experiments) of aperture area (opening area in the membrane) are shown for the air-magnetic fluid interface and oil-magnetic fluid interface, respectively. As seen in Fig. 14, for the air-magnetic fluid interface case, when the magnetic field intensity H_z^* is decreased from point [1] (to which the corresponding image is Fig. 15a) to point [2], the abrupt opening of membrane occurs suddenly at point [2]. After the abrupt opening of membrane at point [2], the aperture area appeared at point [3] (to which the corresponding image is Fig. 15b). Further decrease of the magnetic field intensity H_z^* to point [4] yields the maximum aperture area, as shown in Fig. 15c. Decreasing the magnetic field intensity from point [4] can cause the sustained membrane to flow away, breaking up its shape. Thus, from point [4] the magnetic field intensity is then increased to the same point [3], where the same aperture area as in the decreasing order of H_z^* as shown in Fig. 15b was found. Further increase of the magnetic field intensity up to point [5] caused the aperture area to close and block the test section completely. In Fig. 15d, the image of the aperture area for H_z^* near to point [5] is displayed. The aperture area was kept closed for further increase of the magnetic field intensity toward the beginning point [1]. From this result it is seen that there exists the hysteresis loop for variation of aperture area in the case of air-magnetic fluid interface. The stage of membrane formation between points [1] to [2] (and closer to the point [2]) was found to be somewhat different from other aperture images (such as shown in Figs. 15b, 15c, and 15d). An interference pattern appeared on the thin membrane between the points before rupturing. From the visual observation the hysteresis was caused by the instability of membrane, which is likewise observed in the rupturing phenomena of a soap film.[15] In the case of the air-magnetic fluid interface, the surfactant contained in the water-based magnetic fluid (W-40) might have played an important role in the forming of the membrane film. The surfactant of the water-based magnetic fluid (W-40) might act the same as an ionic surfactant in a soap film.[15]

On the contrary, in the case of the oil-magnetic fluid interface there was no obvious hysteresis phenomenon observed. As seen in Fig. 14, similarly decreasing the magnetic field intensity, starting from point [1] (which corresponds to the image of the aperture area in Fig. 16a) to point [2′], caused the aperture area to open at point [2′], where a pin-point lighting image appeared at the moment of opening, and there was no abrupt opening observed at point [2′]. Decreasing the magnetic field intensity from point [2′] to [3′] kept the aperture area opening wider; an image of the aperture area between point [2′] to [3′] is displayed in Fig. 16b. After reaching the maximum opening of aperture area, at point [3′] (Fig. 16c), the magnetic field intensity was then increased, similar to the case of air-magnetic fluid interface case, to point [4′], where the aperture area closed and blocked the test section completely. The aperture area was kept closed for further increase of the magnetic field intensity toward the beginning point [1]. From the results of oil-magnetic fluid interface, the difference of points [2′] and [4′] is minimal, that is, within measuring uncertainty. Therefore, there would be no clear hysteresis loop observed in the case of oil-magnetic fluid interface within the limitation of measuring aperture area with the video recording method. Thus, it is speculated, in the case of oil-magnetic fluid interface, that there was no substantial effect caused by the surfactant of the water-based magnetic fluid (W-40) between the oil interface.

Finally, it should be stressed that in controlling aperture area a choice of the contact fluid to magnetic fluid is important because hysteresis phenomenon might happen when the magnetic field intensity is varied by descending order or ascending order, depending upon the pass. No prediction for the hysteresis phenomena was achieved in the present study. Highly nonlinear bifurcation analysis would be required, and this is not in the scope of the present study. We will discuss these problems in future studies.

V. Conclusions

Experiments and numerical calculations were conducted to obtain the basic characteristics of membrane formation process, where a volume of magnetic fluid is sustained in a portion of pipe with an imposed magnetic field. From the results of the experiment and accompanying numerical analysis, the following conclusions were drawn:

1) The formation of membrane and variation of aperture area are strongly affected by the volume of the sustained magnetic fluid, intensity of imposed magnetic field, and contact fluids used with the magnetic fluid.

2) The interfacial formation process of a membrane can be presented well by the static force balance between the magnetic body force, the gravitational force, and the surface tension force at the contact point with a solid wall.

3) In variation of aperture area strong hysteresis phenomena exist in the case of an air-magnetic fluid interface. The phenomena could be caused by the effect of the surfactant similar to the soap film rupture phenomena.

Acknowledgment

This work was partly supported by a Grant-in-Aid for Scientific Research (C) from the Ministry of Education, Culture, Sports, Science and Technology, Japan.

References

[1]Rosensweig, R. E., "Cambridge Monographs on Mechanics and Applied Mathematics," *Ferrohydrodynamics*, 1st ed., Cambridge Univ. Press, Cambridge, England, U.K., 1985, pp. 142–146.

[2]Cowley, M. D., and Rosensweig, R. E., "The Interfacial Stability of a Ferromagnetic," *Journal of Fluid Mechanics*, Vol. 30, Pt. 4, 1967, p. 671.

[3]Berkovsky, B. M., *Magnetic Fluids Engineering Applications*, 1st ed., Oxford Univ. Press, New York, 1993, pp. 214–228.

[4]Blums, E., Cebers, A., and Maiorov, M. M., *Magnetic Fluids*, 1st ed., Walter de Gruyter, New York, 1997, pp. 343–375.

[5]Bashtovoy, V. G., Berkovsky, B. M., and Vislovich, A. N., *Introduction to Thermomechanics of Magnetic Fluids*, Hemisphere, Washington, DC, 1988, pp. 108–110.

[6]Alexander, R., and Reinhard, R., "Experiments on the Breakup of a Liquid Bridge of Magnetic Fluid," *Journal of Magnetism and Magnetic Materials*, Vol. 201, 1999, pp. 324–327.

[7]Kozhevnikov, V. M., and Malsugenov, O. V., "Research of Electrical and Geometrical Parameters of an Interelectrode Cross Connection of a Magnetic Fluid," *Book of Abstracts, 9th International Conference on Magnetic Fluids*, ZARM, Bremen, Germany, 2001, pp. 9, 10.

[8]Corriel, S. R., Hardy, S. C., and Cordes, M. R., "Stability of Liquid Zones," *Journal of Colloid and Interface Science*, Vol. 60, 1977, pp. 126–136.

[9]Meseguer, J., "The Breaking of Axisymmetric Slender Liquid Bridges," *Journal of Fluid Mechanics*, Vol. 130, 1983, pp. 123–151.

[10]Sanz, A., and Martinez, I., "Minimum Volume for a Liquid Bridge Between Equal Disks," *Journal of Colloid and Interface Science*, Vol. 93, 1983, pp. 235–240.

[11]Zhu, Z., Ge, P., Hou, C., Chen, D., and Li, C., "Stable Shape of Crystal Growth Face in Crystallization from Solution Under Microgravity," *Journal of Crystal Growth*, Vol. 224, No. 1/2, 2001, pp. 155–164.

[12]Ohaba, M., Sugimoto, T., Sawada, T., Sudo, S., and Takahashi, T., "Oscillations of Magnetic Liquid Columns Subject to Random Vibration," *Journal of Magnetism and Magnetic Materials*, Vol. 201, 1999, pp. 293–296.

[13]Berkovsky, B. M., Medvedev, V. F., and Krakov, M. S., *Magnetic Fluids*, Oxford Univ. Press, Oxford, 1993, pp. 26–30.

[14]Chantrell, R. W., Popplewell, J., and Charles, S. W., "Measurements of Particle Size Distribution Parameters in Ferrofluids," *IEEE Transactions on Magnetics*, Vol. 14, No. 5, 1978, pp. 975–977.

[15]Jacob, N. I., *Intermolecular and Surface Forces*, 2nd ed., Academic Press, London, 1992; Asakura Book Corp., Tokyo, 1996, pp. 301–325 (Japanese translation).